ELSEVIER

Journal of Nuclear Materials 304 (2002) 1–7

journal of nuclear materials

www.elsevier.com/locate/jnucmat

Helium bubble formation in 800 MeV proton-irradiated 304L stainless steel and alloy 718 during post-irradiation annealing

J. Chen [a,*], S. Romanzetti [b], W.F. Sommer [c], H. Ullmaier [a]

[a] *Institut für Festkörperforschung und Projekt ESS, Forschungszentrum Jülich, D-52425 Jülich, Germany*
[b] *INFM Unit of Ancona, I-60131 Ancona, Italy*
[c] *APT/TPO, MS H809, Los Alamos National Laboratory, Los Alamos, NM 87545, USA*

Received 28 January 2002; accepted 10 May 2002

Abstract

The bubble formation in AISI 304L and Alloy 718 irradiated with 800 MeV protons and annealed at temperatures up to 1100 °C has been studied by TEM. The specimens were obtained from spent target components of the LANSCE facility at the Los Alamos National Laboratory. In this and other spallation sources high concentrations of helium are generated concurrent with the displacement damage. In the specimens irradiated with around 3×10^{25} p/m^2 (≈8.4 dpa), first visible bubbles appeared at 700 °C in Alloy 718 and at 800 °C in 304L stainless steel, respectively. Two temperature regions with different coarsening mechanisms could be identified and interpreted as bubble migration and coalescence at lower temperatures and Ostwald ripening at higher temperatures. From the measured bubble densities and size distributions, He concentrations were determined and compared to values obtained by release and nuclear reaction measurements, respectively.

1. Introduction

AISI 304L and Alloy 718 are two candidates for structural materials in the targets of future high-power spallation neutron sources. AISI 304L is an austenitic stainless steel with low carbon content showing good corrosion resistance and high initial ductility. Alloy 718 is a nickel base alloy with high strength and corrosion resistance up to high temperatures. However, the degradation of their mechanical properties by displacement damage and gas transmutation products such as helium is one of the severe issues for their application and lifetime. In future high-power spallation neutron sources such as European Spallation Source (ESS) [1] in Europe and Spallation Neutron Source (SNS) [2] in the USA, the beam window and the target structural materials which are in the proton beam are subject to much higher helium production rates than in a fast fission and fusion environment. The ratio of produced helium to displacements (He/dpa), which is used to indicate the relative importance of helium effects in nuclear materials, is around 0.5, 10 and 150 appm/dpa in steel for fast fission, fusion and spallation, respectively. This means that almost 1 at.% helium would be accumulated in one year of full power operation of ESS in steels. To predetermine the lifetime of spallation targets, a Water-Degrader made of Alloy 718 and AISI 304L irradiated with 800 MeV protons in the Los Alamos Neutron Science Centre (LANSCE) was investigated jointly by Forschungszentrum Jülich in Germany and Paul Scherrer Institut in Switzerland. Results on the changes in mechanical properties and microstructure of materials in the mixed proton and spallation neutron spectra have been reported earlier [3–6].

In this paper we present transmission electron microscopy (TEM) observations of the development of helium bubbles upon post-irradiation annealing. In the materials considered, bubbles of sizes resolvable in TEM

* Corresponding author. Tel.: +49-2461 612 473; fax: +49-2461 614 413.
E-mail address: j.chen@fz-juelich.de (J. Chen).

0022-3115/02/$ - see front matter
PII: S0022-3115(02)00874-7

appear at annealing temperatures which are above the values anticipated in spallation sources employing liquid Hg targets. Nevertheless, studies of this kind yield information on bubble formation and coarsening, from which parameters can be extracted which are needed for modeling helium effects in general. Furthermore, the quantitative determination of bubble size distributions and densities yields helium concentrations which can be compared with values obtained from degassing and nuclear reaction experiments.

2. Experimental

304 L and Alloy 718 samples were cut from a LANSCE Water-Degrader which was in operation from 1988 to 1993 and irradiated by 800 MeV protons with a total charge of 5.3 Ah at a maximum temperature of 250 °C. The proton fluence distribution was determined from gamma-scans giving a fluence of about 2.9×10^{25} p/m^2 in the beam center which corresponds to a displacement dose of 8.4 dpa. The detailed information describing of the LANSCE Water-Degrader, the initial heat treatment of the materials and the irradiation conditions is found in [3,4].

The samples cut from the Water-Degrader and used in this study experienced proton fluences of about 2.9×10^{25} and 2.7×10^{25} p/m^2 for 304L and Alloy 718, respectively. TEM specimens of 2.3 mm in diameter and 0.1 mm in thickness were used in the present investigation. Post-irradiation annealing was performed isothermally in vacuum better than 10^{-4} Pa at temperatures from 700 to 1100 °C for 304L and from 600 to 1000 °C for Alloy 718, for 1 h. Afterwards, the specimens were polished electrochemically with a solution of 5 vol.% perchloric acid and 95 vol.% ethanol at a temperature of −20 °C and a current of 140 mA. TEM examinations were conducted with a Philips TEM430 with an operating voltage of 300 kV. The bubbles were imaged in phase contrast and histograms of the bubble radii r_b were obtained with a particle size analyzer Zeiss TGA-10. For the evaluation of bubble densities, c_b, the foil thickness was determined by the contamination spike technique. The typical precision of this method is about 10%. The concentration of helium accumulated in bubbles, c_{He}, was estimated using Trinkaus [7] equation of state for helium and assuming equilibrium bubbles, i.e. $p_{He} = 2\gamma/r_b$ where p_{He} is the gas pressure and γ is the surface energy.

3. Results

3.1. AISI 304L

The as-irradiated specimens were found to contain a dense population of 'black-dots', and sessile Frank loops having a habit plane of {1 1 1}. The average sizes of the 'black-dots' and Frank loops are 2 and 23 nm, respectively. No visible bubbles were detected by TEM in the as-irradiated samples and after post-annealing at 700 °C. The main change of microstructure in the sample annealed at 700 °C was that 'black-dots' and Frank loops disappeared and a dislocation network had formed. Starting at 810 °C, a dense population of bubbles was observed. These microstructural changes with increasing

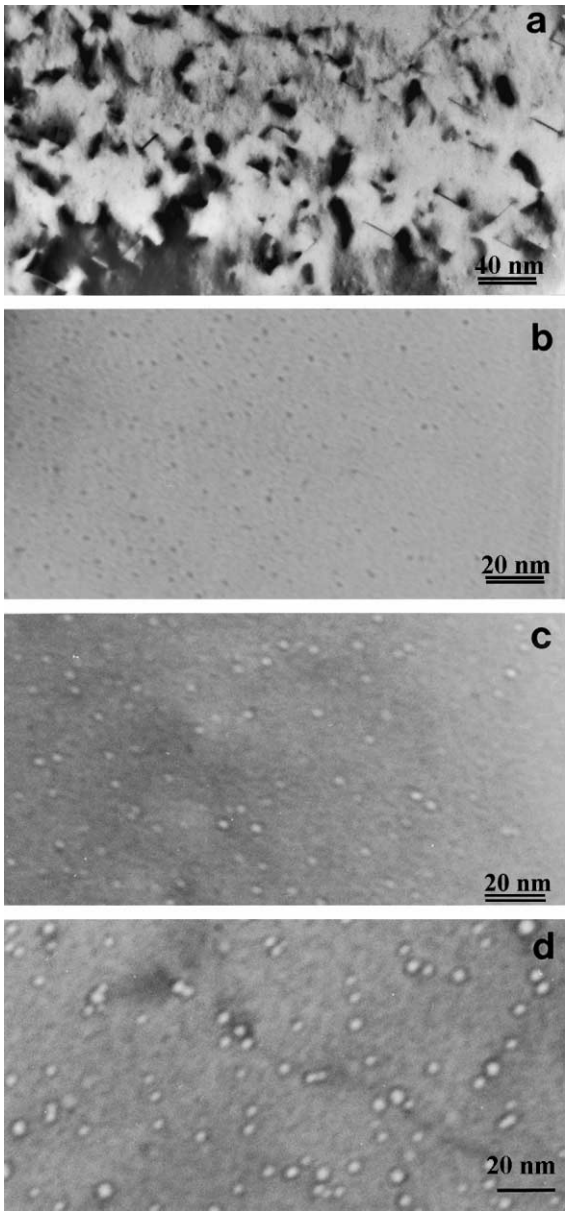

Fig. 1. Micrographs of 304L stainless steel irradiated to 8.4 dpa at $\leqslant$ 250 °C, (a) as irradiated (BF image with B(1 1 0), g(0 0 2)), (b) annealed at 810 °C (over-focal image), (c) at 900 °C (under-focal image) and (d) at 1000 °C (under-focal image) for 1 h in the bulk of a grain.

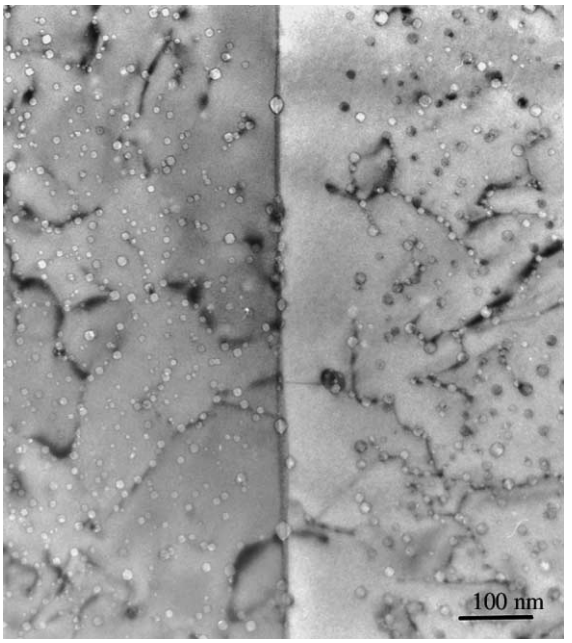

Fig. 2. Bubble arrangement in 304L stainless steel irradiated to 8.4 dpa and annealed at 1100 °C for 1 h.

temperature are shown in Figs. 1 and 2. Two bubble size distributions are given in Fig. 3. The bubbles are distributed fairly uniformly throughout the grain interiors at first glance. But observing more closely, one finds that most of the bubbles are attached to dislocations. The bubbles on the grain boundaries were bigger than in the grain interior. A denuded zone was formed adjacent to the grain boundaries. The width of denuded zone depends strongly on the orientation of the grain boundaries (see Fig. 2). However, the present study is focused on the grain interior. Here the mean bubble diameter is increasing from 1.48 nm at 810 °C to 7.24 nm at 1100 °C. On the other hand, the bubble density is decreasing from 2.0×10^{23} m^{-3} at 810 °C to 9.4×10^{21} m^{-3} at 1100 °C.

3.2. Alloy 718

A remarkable change of Alloy 718 irradiated to 7.8 dpa was the disappearance of γ' and γ'' phases. The γ' and γ'' superlattice diffraction spots, clearly evident for unirradiated samples, were absent after irradiation. As in the case of 304L, Frank loops on {1 1 1} habit planes and an average diameter of 15 nm were formed (Fig. 4(a)). These results has been reported early in Refs. [3,8]. Examination of the samples as-irradiated and annealed at 600 °C showed no bubble formation. Starting at 700 °C, 100 °C earlier than in 304L, a dense population of bubbles was observed (Fig. 4(b)). Most of the bubbles were attached to dislocation and precipitates. The mean bubble diameter increased from 1.8 nm at 700 °C to 14.7

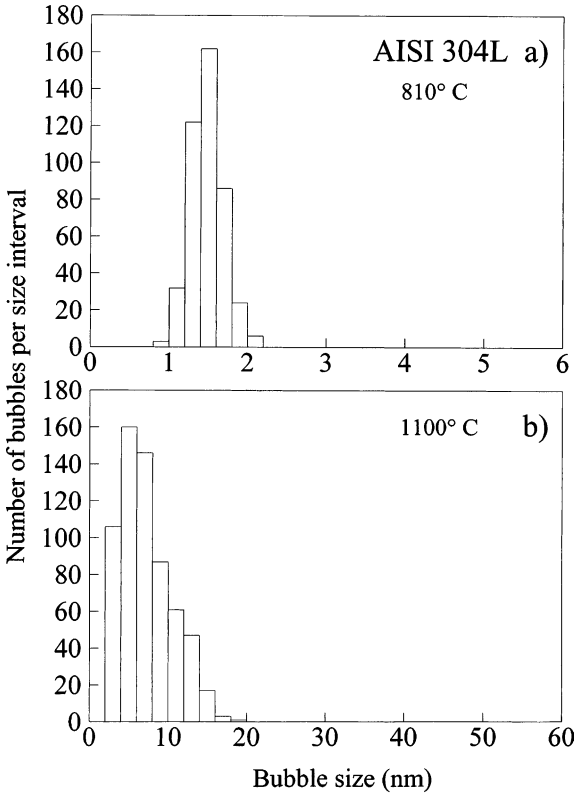

Fig. 3. Size distribution of helium bubbles in the grain interior of 304L stainless steel irradiated to 8.4 dpa and annealed at (a) 810 °C and (b) 1100 °C.

nm at 1000 °C and the bubble density decreased from 1.1×10^{23} m^{-3} at 700 °C to 1.3×10^{21} m^{-3} at 1000 °C. Two examples of size distributions are shown in Fig. 5. Besides bubble formation, the γ' and γ'' precipitates reappeared at annealing temperatures of 600, 700, 800 and 900 °C but not at 1000 °C. Moreover, the Frank loops grew with increasing annealing temperature up to 700 °C where a dislocation network had already formed in 304L. Since the main aim of this paper is to investigate the bubble formation, details of the loop and precipitate evolution during annealing will not be discussed further.

4. Discussion and conclusion

During annealing at elevated temperatures, small He–V complexes produced by cold-irradiation coarsen and form bubble nuclei. Further coarsening of these bubble nuclei will occur either by bubble migration and coalescence (MC) or by thermal resolution and reabsorption of gas atoms and vacancies (Ostwald ripening, OR) [9,10]. To help our discussion we list here the different coarsening models and the respective dependencies on annealing time t and temperature T. In the case

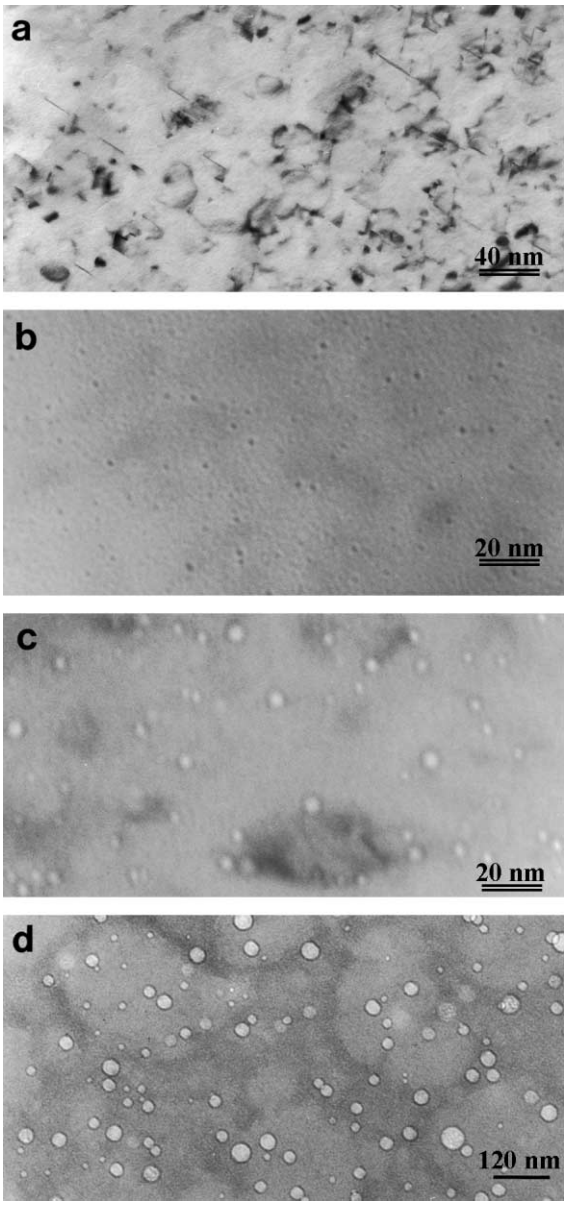

Fig. 4. Micrographs of Alloy 718 irradiated to 7.8 dpa at $\leqslant 250$ °C, (a) as irradiated (BF image with B(1 1 0), g(0 0 2)), (b) annealed at 700 °C (over-focal image), (c) at 810 °C (under-focal image) and (d) at 1000 °C (under-focal image) for 1 h in the grain interior.

of MC, bubble migration depends on the prevailing diffusion mechanism such as surface diffusion (SD), volume diffusion (VD) or vapour transport (VT) through the bubble. The increase in the mean bubble radius $\bar{r}_b$ with annealing time t due to MC may be approximately described by [7,9]

$$\bar{r}_b^n \propto D_X c_{He} t, \tag{1}$$

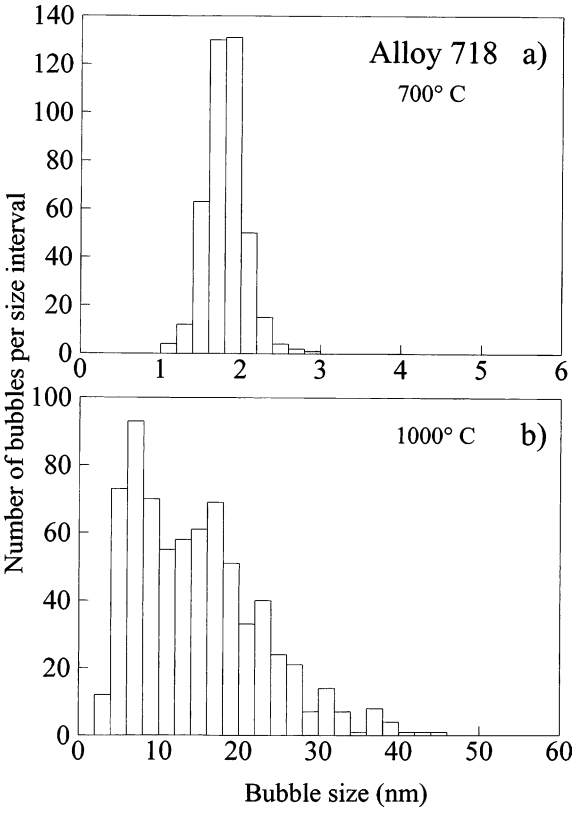

Fig. 5. Size distribution of helium bubble in the grain interior of Alloy 718 irradiated to 7.8 dpa and annealed at (a) 700 °C and (b) 1000 °C.

where c_{He} is helium concentration and D_X is the diffusion coefficient of the underlying diffusion mechanism ($x =$ SD, VD or VT for surface diffusion, volume diffusion or volume transport through the bubble, respectively). If we assume that the bubble migration is SD controlled, the exponent $n = 5$ for equilibrium bubbles and $n = 6$ for constant total volume of the bubbles (i.e. incompressible helium). If we assume that the bubble migration is VD controlled, $n = 4$ or 5 for equilibrium bubbles and constant volume, respectively. Finally, $n = 3$ or 5 for equilibrium bubbles and constant volume, respectively, in the case of vapour transport MC.

In the case of OR, the bubble coarsening can be gas dissociation or vacancy dissociation controlled, depending on which process is more difficult. The mean radius of bubbles containing ideal gas increases with time as [7,11]

$$\bar{r}_b^2 \propto kTD_{He}K_{He}t \tag{2}$$

for helium dissociation controlled and

$$\bar{r}_b^3 \propto (\gamma\Omega/kT)D_V t \tag{3}$$

for vacancy dissociation controlled bubble OR.

Here D_{He} and D_V are the He and vacancy diffusion coefficient, respectively, kT is the thermal energy, K_{He} is the He solubility coefficient, γ is the surface energy and Ω is the atomic volume of the matrix.

According to Eqs. (1)–(3) the apparent activation energy of the $\bar{r}_b$ evolution, E_r, reflects the activation energy of the diffusion process controlling MC or of the dissociation process controlling OR, respectively. More in detail, $E_{SD} = 5E_r$ for equilibrium bubbles or $E_{SD} = 6E_r$ for constant volume of He in the case of SD-controlled bubble MC (where E_{SD} is the SD energy). In the case of He atom and vacancy dissociation controlled OR, $E_{He}^{diss} = 2E_r$ and $E_V^{diss} = 3E_r$, respectively (where E_{He}^{diss} and E_V^{diss} are the activation energies of He atom and vacancy dissociation from a bubble, respectively).

The temperature dependences of the observed bubble sizes and densities in 304L and Alloy 718 are given in Fig. 6. Our experimental data are characterized by two distinctly different regimes. The transition temperatures, T_r, are around 1050 and 750 °C in 304L and Alloy 718, respectively. Firstly, we discuss the possible growth mechanism of the bubbles in 304L. The apparent activation energy (E_r), deduced from the temperature dependence of the mean bubble radius in the low-temperature regime, is 0.29 ± 0.015 eV. This value is not far from the value of $E_r = 0.25$ eV deduced from the data in the low-temperature branch of the bubbles in the grain interior of Ni [13]. Such a low value of the apparent activation energy suggests that SD-controlled bubble MC is the prevailing growth mechanism yielding $E_{SD} = (5–6) \bullet E_r = 1.45 \pm 0.07–1.74 \pm 0.09$ eV which is in the range expected for E_{SD} in Ni (<2 eV). There are not sufficient experimental points to determine the apparent activation energy of the high-temperature branch, but a lower limit of 1.7 eV can nevertheless be given. Probably by coincidence, this value is exactly the same as reported earlier for 316L [12], a quite similar material, but implanted to lower helium concentrations (100 appm) and annealed to longer times (185 h). According to the theoretical analysis in Ref. [12], He atom dissociation controlled OR with $E_{He}^{diss} = 3.5$ eV is the prevailing growth mechanism. This value is in good agreement with our data of the higher temperature branch yielding $E_{He}^{diss} = 2E_r = 3.4$ eV.

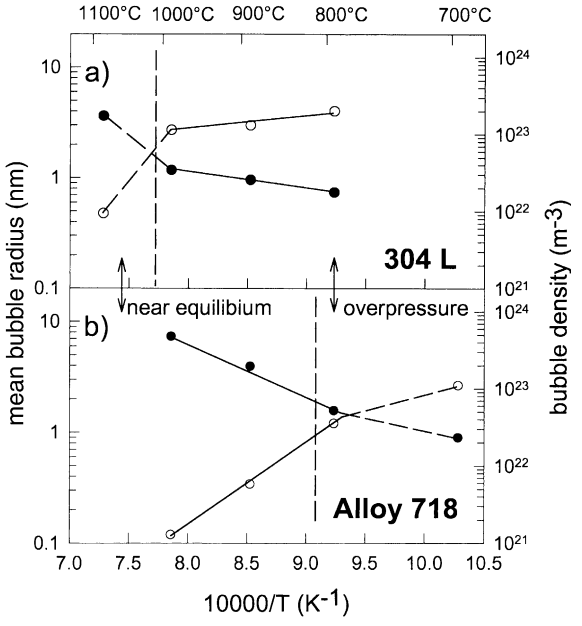

Fig. 6. Mean radii of bubbles (closed symbols) and their densities (open symbols) as a function of the annealing temperature in (a) of 304L with 8.4 dpa and (b) Alloy 718 with 7.8 dpa.

Now we consider Alloy 718. The apparent activation energies are $\leqslant 0.4$ and 1.0 ± 0.1 eV for the low- and high-temperature regime, respectively. Again, lack of sufficient experimental data allows only an upper limit, but in this case for the low-temperature regime. The high-temperature value of 1.0 eV agrees with results on bubbles near the surface and grain boundaries which have an apparent activation energy of 1.1 eV in He-implanted Ni [13]. In contrast to Ni, the high overpressure of bubbles in the bulk can be relaxed by absorption of vacancies in Alloy 718 already at 810 °C. If vacancy controlled OR governs their coarsening, a dissociation energy $E_V^{diss} = 3.0 \pm 0.3$ eV is obtained which is in good agreement with $E_V = 2.9$ eV [14], the self-diffusion energy in Ni.

The helium concentrations in the samples can be calculated from measured bubble densities and size distributions assuming that the helium gas in the bubbles is under a pressure in equilibrium with the surface tension and that it obeys the equation of state suggested by Trinkaus [7]. More in detail, the helium content was determined for each size class measured on the particle size analyzer. These values were then multiplied by the frequency factor for the size class and summed over all size classes. Values of surface energies used in the calculations were taken from Ref. [15] for 304L and estimated to be 2 N/m for Alloy 718. The results are given in Table 1. It is not surprising that the calculated helium contents at temperatures lower than or close to T_r are much less than at high temperatures. There are two possible reasons for that: (a) not all helium atoms are in the visible bubbles, and (b) the bubbles are overpressurized. Our TEM has a resolution limit of about 1 nm for bubble observation which means that the first reason could only apply to the samples of 304L at 810 °C and Alloy 718 at 700 °C (cf. Figs. 3 and 5). Gas pressures exceeding the equilibrium values by about 3 GPa have indeed been measured directly by small angle neutron scattering on bubbles in Ni [16] and FeCrNi [17] annealed at 700 °C. However, the pressure in the bubbles was found to be close to its equilibrium value at

Table 1
Summary of bubble parameters and calculated apparent helium concentrations

T_{ann} (°C)	$\bar{r}_b$ (nm)	c_b (m^{-3})	γ (N/m)	c_{He} (appm)	σ_{He} (barn)	He/dpa (appm/dpa)
304L (8.4 dpa)						
810	0.74	2.0×10^{23}	2.63	385	–	
900	0.96	1.3×10^{23}	2.44	464	–	
1000	1.18	1.1×10^{23}	2.25	593	–	
1100[a]	3.62	9.4×10^{21}	2.05	987	0.34	120
Alloy 718 (7.8 dpa)						
700	0.90	1.1×10^{23}	2	348	–	
810	1.58	3.6×10^{22}	2	400	–	
900[a]	3.96	5.9×10^{21}	2	826	0.31	106
1000[a]	7.37	1.3×10^{21}	2	793	0.30	103

[a] Equilibrium bubbles formed.

temperatures higher than T_r in Ni [13] and 316L [12]. Our experiment showed that the ratio of the exponents between the $\bar{r}_b$ and c_b at higher temperatures in both 304L and Alloy 718 is about −2.2 which is rather close to −2, indicating equilibrium bubbles filled with ideal gas. Therefore, the values determined in the high-temperature branches, i.e. at 1100 °C for 304L and 900 and 1000 °C for Alloy 718 (see Table 1) should yield a reasonable estimate of the helium content. Dividing the obtained values of 987 appm for 304L and 810 appm for Alloy 718 by the proton fluences of 2.9×10^{25} and 2.7×10^{25} m^{-2}, respectively, yield a mean value of the cross section for helium production by 760 MeV protons of 0.34 barn for 304L and 0.30 barn for Alloy 718. Helium release measurements on specimens irradiated under the same conditions yield 0.58 barn for 304L and 0.52 barn for Alloy 718 [18]. Nuclear reaction measurements within the NESSI collaboration give a cross-section of 0.4 barn for 800 MeV protons in Fe [19]. Considering the large uncertainties inherent in each of the three techniques, the agreement of the data is satisfactory and shows that the helium production in medium-Z elements in a spallation environment can be estimated within an uncertainty of ±25%.

In summary, the following conclusion can be drawn from the present study on helium bubble formation during post-irradiation annealing of specimens irradiated by high-energy protons.

(1) In 304L first visible bubbles appears at 810 °C. Activation energy analysis suggests that they coarsen by surface diffusion controlled migration and coalescence ($E_{SD} = 1.74 \pm 0.09$ eV) up to a transition temperature T_r of around 1050 °C and by He dissociation controlled Ostwald ripening ($E_{He}^{diss} = 3.4$ eV) at higher temperatures.
(2) In Alloy 718 first visible bubble appears at 700 °C. For temperatures above $T_r \approx 750$ °C they are likely to coarsen by vacancy dissociation controlled Ostwald ripening ($E_V^{diss} = 3.0 \pm 0.3$ eV).
(3) Assuming that the bubbles are close to thermal equilibrium at the highest temperatures applied, the helium content in the specimens can be determined using the measured bubble size distributions and densities for He production in Fe/Ni base alloys by 760 MeV protons of about 0.32 barn which is in reasonable agreement with helium release measurement and data from nuclear reaction experiments.

Acknowledgements

The authors are grateful to all the staff members of the Hot Cells of the Forschungszentrum Jülich for their support in specimen handling and preparation.

References

[1] ESS – A Next Generation Neutron Source for Europe, vol. 1–3, ESS Council I. Kjems, chairman 1997, ISBN 090 2376 500.
[2] Spallation Neutron Source at Oak Ridge, TN, USA. www.sns.gov/documentation/pubs.htm.
[3] F. Carsughi, H. Derz, P. Ferguson, G. Pott, W.F. Sommer, H. Ullmaier, J. Nucl. Mater. 264 (1999) 78.
[4] J. Chen, Y. Dai, F. Carsughi, W.F. Sommer, G.S. Bauer, H. Ullmaier, J. Nucl. Mater. 275 (1999) 115.
[5] Y. Dai, X. Jia, J.C. Chen, W.F. Sommer, M. Victoria, G.S. Bauer, J. Nucl. Mater. 296 (2001) 174.
[6] M.R. James, S.A. Maloy, F.D. Gac, W.F. Sommer, J. Chen, H. Ullmaier, J. Nucl. Mater. 296 (2001) 139.
[7] H. Trinkaus, Radiat. Eff. 78 (1983) 189.
[8] B.H. Sencer, G.M. Bond, F.A. Garner, M.L. Hamilton, S.A. Maloy, W.F. Sommer, J. Nucl. Mater. 296 (2001) 145.
[9] P.J. Goodhew, S.K. Tyler, Proc. Roy. Soc. London A 377 (1981) 151.
[10] B.N. Sigh, H. Trinkaus, J. Nucl. Mater. 186 (1992) 153.
[11] A.J. Markworth, Metall. Trans. 4 (1973) 2651.

[12] J. Rothaut, H. Schröder, H. Ullmaier, Philos. Mag. 47 (1983) 781.
[13] V.N. Chernikov, H. Trinkaus, H. Ullmaier, J. Nucl. Mater. 250 (1997) 103.
[14] O. Madelung (Ed.), Landolt-Börnstein, N.S. vol. III 25, Springer, Berlin, 1991, p. 243.
[15] L.E. Murr, G.I. Wong, R.J. Horylev, Acta Metall. 21 (1973) 595.
[16] L. Qiang, W. Kesternich, H. Schröder, D. Schwahn, H. Ullmaier, Acta Metall. Mater. 38 (1990) 2383.
[17] F. Carsughi, W. Kesternich, D. Schwahn, H. Ullmaier, J. Nucl. Mater. 191–194 (1992) 1284.
[18] F.A. Garner, B.M. Oliver, L.R. Greenwood, M.R. James, P.D. Ferguson, S.A. Maloy, W.F. Sommer, J. Nucl. Mater. 296 (2001) 66.
[19] D. Hilscher, C.-M. Herbach, U. Jahnke, V. Tishchenko, M. Enke, D. Filges, F. Goldenbaum, R.-D. Neef, K. Nünighoff, N. Paul, H. Schaal, G. Sterzenbach, A. Letourneau, A. Böhm, J. Galin, B. Lott, A. Péghaire, L. Pienkowski, J. Nucl. Mater. 296 (2001) 83.